Title
Dispersion-free continuum two-dimensional electronic spectrometer.

Journal
Applied Optics, 53(9)

ISSN
0003-6935

Authors
Zheng, Haibin
Caram, Justin R
Dahlberg, Peter D
et al.

Publication Date
2014-03-20

DOI
10.1364/ao.53.001909

Peer reviewed

Dispersion-free continuum two-dimensional electronic spectrometer

Haibin Zheng,[1,†] Justin R. Caram,[1,†] Peter D. Dahlberg,[2] Brian S. Rolczynski,[1] Subha Viswanathan,[1] Dmitriy S. Dolzhnikov,[3] Amir Khadivi,[1] Dmitri V. Talapin,[3] and Gregory S. Engel[1,*]

[1]Department of Chemistry, The James Franck Institute, and The Institute for Biophysical Dynamics, The University of Chicago, Chicago, Illinois 60637, USA

[2]Program in the Biophysical Sciences, The James Franck Institute, and The Institute for Biophysical Dynamics, The University of Chicago, Chicago, Illinois 60637, USA

[3]Department of Chemistry and The James Franck Institute, The University of Chicago, Chicago, Illinois 60637, USA

*Corresponding author: gsengel@uchicago.edu

Received 7 November 2013; revised 3 February 2014; accepted 6 February 2014; posted 12 February 2014 (Doc. ID 200919); published 19 March 2014

Electronic dynamics span broad energy scales with ultrafast time constants in the condensed phase. Two-dimensional (2D) electronic spectroscopy permits the study of these dynamics with simultaneous resolution in both frequency and time. In practice, this technique is sensitive to changes in nonlinear dispersion in the laser pulses as time delays are varied during the experiment. We have developed a 2D spectrometer that uses broadband continuum generated in argon as the light source. Using this visible light in phase-sensitive optical experiments presents new challenges in implementation. We demonstrate all-reflective interferometric delays using angled stages. Upon selecting an ~180 nm window of the available bandwidth at ~10 fs compression, we probe the nonlinear response of broadly absorbing CdSe quantum dots and electronic transitions of Chlorophyll *a*.

OCIS codes: (320.7150) Ultrafast spectroscopy; (300.6550) Spectroscopy, visible; (300.2570) Four-wave mixing.

http://dx.doi.org/10.1364/AO.53.001909

1. Introduction

Two-dimensional electronic spectroscopy (2DES) probes photo-initiated electronic dynamics on ultrafast timescales [1–4]. It has been applied to study systems including spectral diffusion [1,5,6], photosynthetic light-harvesting [7–14], semiconducting nanocrystals [15–18] and atomic vapors [19–22]. 2DES improves resolution compared to pump–probe spectroscopies by separating homogenous and inhomogeneous broadening along distinct spectral axes [23]. The resulting 2D maps correlate excitation at a specific energy with the fate of that excitation across the entire excitation window. This approach decouples the pulse bandwidth from the frequency resolution of the experiment, which is ultimately determined by the molecular response. Thus, 2DES can exploit spectrally broad, sub-10-fs, ultrafast pulses for pump and probe, while monitoring electronic and vibrational couplings and coherences across diverse chromophores and environments. 2DES accesses detailed dynamical information without the use of multiple spectrally distinct laser pulses. In this work, we describe an all-reflective implementation of 2DES with a single broadband continuum laser source for all interactions, which allows simultaneous interrogation of multiple electronic excited states. We exploit a simple method of obtaining precision time delays using reflective optics and angled translational stages.

1559-128X/14/091909-09$15.00/0

This method allows us to probe materials with ground-state and transient spectral features spanning several hundred nanometers, while limiting nonlinear dispersion. Here, we investigate the multiple excited states in highly distinct chemical systems with important excitonic dynamics, CdSe quantum dots (QDs), and Chlorophyll a (Chl a).

The details of 2DES have been discussed extensively [2–4,24,25]. Briefly, a sequence of three ultrafast laser pulses interacts with the sample with precisely controlled time delays. The first and second pulses interact with a time separation τ (coherence time), during which the system evolves in an optical coherence between the ground and excited states. After the second interaction, the system undergoes evolution in the excited- or ground-state manifolds for a waiting time T, then a third pulse puts the system into a second optical coherence. We then heterodyne the signal emitted in the phase-matched direction $(-\boldsymbol{k_1}+\boldsymbol{k_2}+\boldsymbol{k_3})$ with an attenuated local oscillator (LO) pulse and collect data in the frequency domain using a CCD spectrometer. Interchange between pulses 1 and 2 allows collection of rephasing and nonrephasing spectra, which, taken together, can be phased to generate absorptive or dispersive 2D spectra. Generation of phased 2DES spectra requires optical phase stability between the first two interactions and minimal temporal dispersion among the pulses [26,27].

Several methods have been used to implement the requisite interferometric time delays in 2DES. Timings can be controlled using retroreflectors mounted on sinusoidal encoded or piezoelectric motor stages that move parallel to the direction of beam propagation with control of approximately 6673 fs/mm [28–30]. The accuracy can be further improved by using active phase stabilization [31]. Delays can also be implemented with more precise control (<50 fs/mm) using paired, angled glass wedges, effectively "gearing" the delay [3,4]. The delay between pulses 1 and 2 can also be encoded along a spatial dimension, where multiple time delays are directly imaged on a camera in a single experiment [32,33]. Moreover, delays can be set using spatial light modulators [34] or acousto-optic modulators [19,35–38]. Finally, the Soleil–Babinet compensator has recently been used for generating a time delay between two pulses [39]. In this work, we seek fine temporal resolution across a wide bandwidth without changes in temporal dispersion; therefore, we avoid transmissive optics. As a result, we have designed a simple system to control the time delay with high resolution, while using all-reflective optics. The use of supercontinuum light sources in 2DES is now allowing access to broader spectral regions and even ultraviolet 2DES [14,17,40–43].

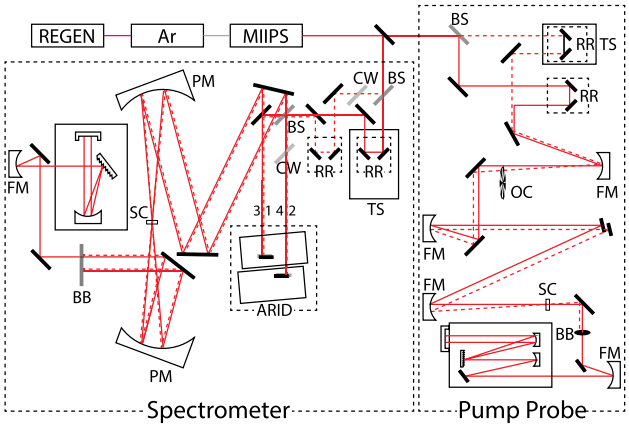

Fig. 1. Experimental implementation for Continuum Two-Dimensional Electronic Spectroscopy (C-2DES): An ultrafast pulse is split into four pulses using beamsplitters (BS); compensating windows (CW) are introduced in each beam to ensure all beams pass through the same amount of glass. A retro-reflector (RR) mounted on a translation stage (TS) introduces the waiting time delay, T. The all-reflective interferometric delay system (ARID) controls the coherence time τ by translating mirrors nearly perpendicular to the incoming beams. An off-axis parabolic mirror (PM) focuses the four beams on the sample cell (SC). The signal field and LO pass through a beam block (BB) and are imaged on a CCD detector. In the accompanying pump–probe experiment, we introduce an optical chopper (OC) to modulate the pump beam.

2. Experiment

A. Two-Dimensional Electronic Spectroscopy

The experimental apparatus is shown in Fig. 1. The 800 nm output of a Coherent Micra Ti:sapphire oscillator was amplified in a Coherent Legend Elite regenerative amplifier to produce a 5 kHz, 4 W, 38 fs FWHM pulse train centered at 800 nm with approximately 35 nm of spectral bandwidth. By focusing the approximately 800 μJ pulse into a 2 m tube filled with 2 atm of argon gas, ultra-broadband pulses spanning from 450 to 900 nm were generated [44–48]. Using a dichroic mirror, light redder than 700 nm is attenuated and the portion spanning 525 to 700 nm (shown in Fig. 2) is then shaped and compressed using the Multiphoton Intrapulse Interference Phase Scan (MIIPS; Biophotonic Solutions, Inc.) method [49,50]. The bandwidth

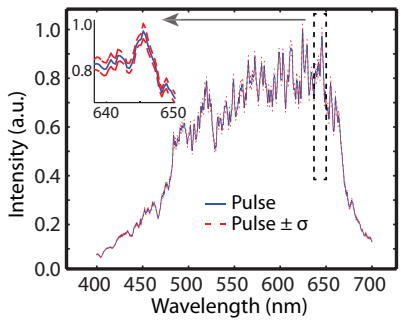

Fig. 2. Stability of supercontinuum source: The white light spectrum from the supercontinuum source (before spectral shaping in the Biophotonics MIIPS system) is shown above (blue, solid). To obtain this spectrum, the supercontinuum is filtered by a dichroic mirror that removes light above 700 nm. The wavelength-dependent fluctuations (red, dashed, $\pm 1\sigma$) measured every 5 s over a 24 min period are ~0.5% across the entire spectrum.

was limited by the grating in the MIIPS system. We compensated for dispersion by optimizing the second-harmonic generation (SHG) signal FWHM at the sample position using the MIIPS. To further validate the instrument, we performed transient grating frequency-resolved optical gating (TG-FROG) in neat methanol to characterize the temporal behavior (shown in Fig. 3) [51–53]. The pulse duration was measured with MIIPS at the sample position to be ~8 fs [as shown in the inset of Fig. 3(c)], with <5% deviation from the transform limit. Similar bandwidths and compression can be achieved with noncollinear optical parametric amplification (NOPA) [54,55].

Continuum pulses were split using a set of two beam splitters (BK7 substrate, 3 mm thickness, AR-coated backs). The first beam splitter separates beams 1 and 2 from beams 3 and the LO, and then beams 1 and 2 are delayed using a retroreflector mounted to a motorized linear stage (Aerotech) to set the waiting time. These vertically separated beams are split again using a second beam splitter to generate four equal pulses in a boxcar geometry with 12 mm separation. Each beam propagates through identical amounts of optical glass, including neutral density and corresponding compensation plates. The coherence time was controlled by the purely reflective delay system. Our approach translates a flat mirror aligned to reflect the level incoming beam upward at a small angle. The mirror is translated nearly perpendicular (~0.3 deg horizontally from the plane normal to beam propagation) to the incident beam path. This implementation of a purely reflective delay stage is similar to the four quadrant mirror introduced by Zhang *et al.* [28]. In our implementation, as the position of the incident beam moves along the translating mirror, the optical path length changes slightly, resulting in controllable delay and negligible translation of the outgoing beam. Detailed analysis of the performance of the delay and the effects of translation of the beam will be presented in Section 3.

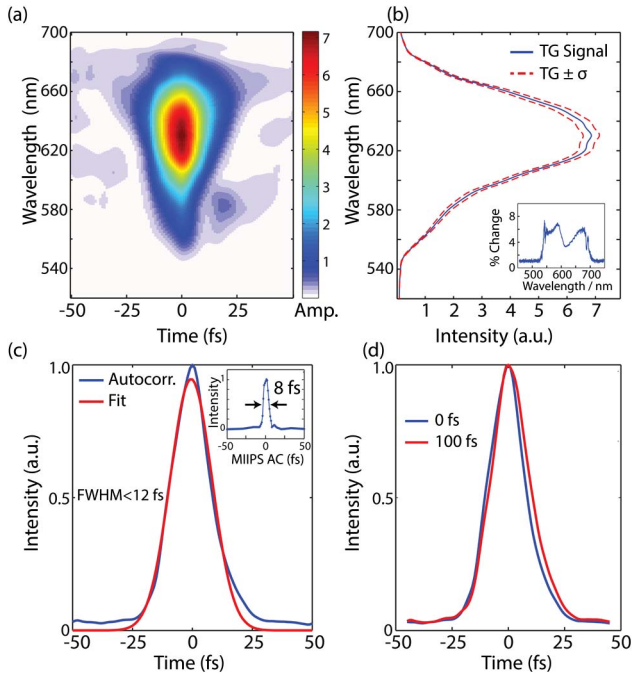

Fig. 3. (a) Representative transient grating frequency-resolved optical gating (TG-FROG) measurements. (b) The TG signal and the wavelength-dependent standard deviation (1σ) when all three pulses are overlapped indicate approximately 0.5% third-order signal stability. The inset shows flat, wavelength-dependent fluctuations. (c) Shown is the sum the TG trace and the fit to a Gaussian function, from which we derive an autocorrelative width of 12 fs. The inset shows the corresponding MIIPS trace with 8 fs width (FWHM). (d) Two autocorrelation traces taken at different delay configurations show that intensity does not change (less than 1% change) when all stages are translated 100 fs (data not individually normalized).

The pulses are then focused to a 100 μm diameter spot on the sample with a 15° off-axis parabolic mirror of 45 cm effective focal length. After recollimation by another parabolic mirror and selection of the phase-matched signal ($-\boldsymbol{k_1}+\boldsymbol{k_2}+\boldsymbol{k_3}$) using a mask, we focus the signal and the LO into a 0.3 m spectrometer (Shamrock, Andor) and camera (Newton, Andor) where it is frequency-resolved and heterodyne-detected. The bandwidth and focal properties satisfy constraints for spatial conditions laid out in previous theoretical studies [56]. Spatial beam translation caused from this delay strategy is measured and characterized below.

For CdSe QD spectra, we use an attenuated pulse energy of 14 nJ/pulse to collect data over a range of coherence times τ from −60 to 80 fs at 1 fs increments and over a range of waiting times T from 0 to 1000 fs in steps of 5 fs. We Fourier transform the resulting interferograms, Fourier interpolate to the time domain [57], and transform over both dimensions to generate a 2D spectrum. We then fit the projected spectrum to separately collected pump–probe data according to the following equation to generate phased 2D spectra for all waiting times:

$$PP(T,\omega_t) = \mathrm{Re}\left\{A\int_{-\infty}^{\infty} S_{2D}(\omega_\tau,T,\omega_t)\exp(i\varphi + i(\omega_t-\omega_0)t_c + i(\omega_t-\omega_0)^2 t_q^2 + i(\omega_\tau-\omega_0)\tau_c)\mathrm{d}\omega_\tau\right\}, \quad (1)$$

where φ is an overall constant phase correction, t_c and τ_c correct for timing between beam 3 and the LO and errors in timing between beams 1 and 2, respectively, and t_q corrects the quadratic nonlinear dispersion arising from the neutral density filter in the LO beam. The quadratic correction term t_q is set to a constant value for all 2D spectra; this value was determined by regression using spectra with $T > 100$ fs where the value was found to be nearly constant. This phasing scheme adds a nonlinear dispersion term and a coherence timing term to the scheme proposed by Brixner *et al.* [4]. The quadratic term should become more important as bandwidth increases. For Chl *a*, the data is acquired

using a pulse energy of 18 nJ/pulse over a range of coherence times from −100 to 150 fs at 1 fs increments and a range of waiting times from 0 to 1000 fs in steps of 5 fs.

B. Transient Absorption

We use separately collected transient absorption spectra to phase each 2D spectrum [4,58–60]. The power is attenuated to achieve a pump pulse of 40–70 nJ/pulse and a probe pulse power of 0.44 nJ. Results are qualitatively consistent with previous broadband pump–probe work performed on these systems [61–63]. A standard delay stage (Aerotech) alters the path length of the pump pulse relative to the probe to generate the temporal delay. An MC2000 optical chopper (Thorlabs, Inc.) synchronized to the regenerative amplifier output modulates the pump pulse at half the laser repetition rate, resulting in every other shot generating a probe or pump–probe spectrum. The pump and probe beams are focused to an approximately 100 μm spot in the sample. The probe and pump–probe signals are then focused into a MicroHR spectrometer (Horiba Scientific). The spectrally resolved probe/pump–probe signals are recorded using a high-speed, line scan Spyder3 camera (Teledyne Dalsa) at 5 kHz synchronized to the output of the regenerative amplifier. During acquisition, we dither the delay stage by 2–4 fs, which effectively eliminates pump–probe heterodyne signals (the signal due to pump scatter heterodyning with the probe beam) while not changing the phase of the third-order transient absorption signal.

3. Discussion

In Fig. 2, we show power stability of our white-light spectrum acquired over 25 min, demonstrating fluctuations of less than 0.5% across the visible range. The phase stability of the instrument was measured by recording a series of interferograms between beams 3 and the LO. Using the method described by Prokhorenko *et al.* [64], we measure phase stability between each pair of beams of $\lambda/75$ at 800 nm over 2.5 h (Fig. 4); this stability is less than the $\lambda/100$ reported by Selig *et al.* [30] using the third-order signal and LO in a passively phase-stabilized configuration geometry that cancels mirror vibrations. One representative interferogram is shown in Fig. 5(a), illustrating the broadband interferogram and relative phase consistency between each beam. We use this interferogram to measure the frequency-dependent dispersion profiles at the sample. To verify that each beam propagates through identical glass, we apply a moving window function Fourier transform across the wavelength dimension, which apodizes the interferogram. In the time-domain, we map the time delay for each wavelength component [Fig. 5(b)]. A flat profile indicates that all frequencies have identical phase profiles at the sample position. We repeated this method for all pulse pairs to ensure compensating windows and neutral density filters are precisely matched.

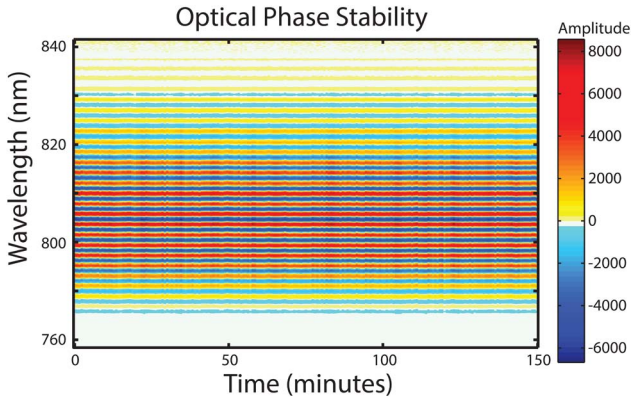

Fig. 4. Optical phase stability between beams 1 and 4, measured every 45 s over 150 min, using the 800 nm pulse from the regenerative amplifier. This data illustrates the mechanical phase stability of the apparatus.

We have designed our reflective delay method to delay each beam while maintaining relative nonlinear dispersive profiles. Each beam reflects off an independent mirror that sets its time delay. Instead of moving mirrors along the direction of beam propagation (as with a retroreflector), we mount the mirrors that set the coherence time on two

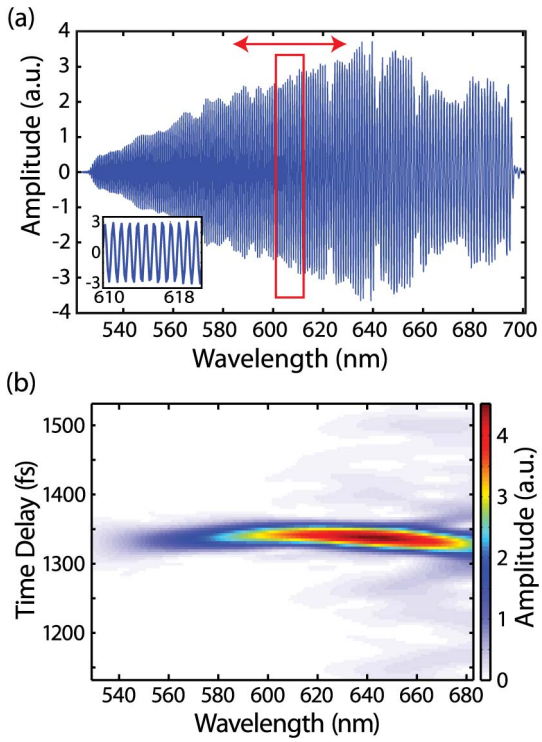

Fig. 5. Characterization of compensating glass. (a) The interferogram of pulse 3 and LO after spectral filtering through the MIIPS compression system. The red box indicates the moving window function over which the Fourier transform is applied to generate the spectrogram below; (b) To illustrate relative dispersive characteristics between pulses, we move the window function shown in (a), to show the time domain signal across different wavelengths. This measure illustrates the relative spectral coherence of the pulse, indicating propagation through similar amounts of glass.

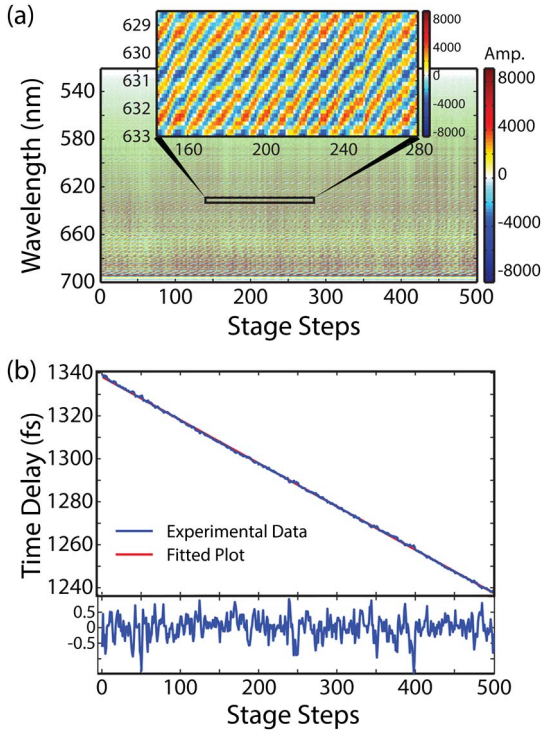

Fig. 6. (a) Interferogram between pulse 2 and LO when scanning pulse 2. The magnified portion indicates the interferometric detail of a representative smaller region. (b) Plot of the measured time delay between pulse 2 and LO at each step as measured by spectral interferometry from the data shown above (blue line). The red line shows the fit to a linear function. We plot the residual below. The standard deviation is ~0.30 fs/step, which is approximately the Fourier-limited resolution given the bandwidth of our laser pulse.

identical translation stages, which move at a small horizontal angle θ relative to the plane normal to beam propagation. By setting the angle, we improve the resolution of the coherence time delay relative to the retroreflectors by a factor of $1/\sin(\theta)$, from 6673 fs/mm to ~35 fs/mm ($\theta \sim 0.3°$). Furthermore, by increasing θ, we may lower the precision of time control, but be able to access a larger temporal range, which is necessary to scan long-lived coherences (such as those accessed by systems with narrow line shapes, like quantum wells and gas vapors). In Fig. 6, we show that this delay can be reliably scanned to generate time delays with 0.25 fs precision using a continuum source. The surface flatness of our optics is specified as $\lambda/10$ at 633 nm, which yields a small error in calibration (~0.2 fs). We have extended Prokhorenko *et al.*'s method [64] to extract phase stability as the mirror moves using the timing extracted in Fig. 5 to show that the stability during scan (including contributions from vibrations, mirror flatness, stage dither, etc.) is better than $\lambda/30$. We believe that the dominant contribution to our phase stability during the scan is the surface flatness of the mirror. Nonetheless, this apparatus yields delays and precision similar to previous passively phase-stabilized techniques, wherein a pair of parallel glass wedges was used to control time delays [32,65]. Each beam travels through a different amount of glass to generate a temporal delay (<50 fs/mm for 1° glass wedges), which provides excellent phase stability but induces nonlinear wavelength-dependent delays, leading to distinct chirp for each beam, which can lead to distorted line shapes and false cross peaks in 2D spectra [66]. The distortion is even more significant when using ultra-broadband white light. For instance, when setting a 200 fs pulse delay using the wedge method, the red edge (700 nm) would be 2.4 fs ahead of blue edge (520 nm). Therefore, all-reflective delay methods provide an avenue to explore longer coherence times, without introducing this nonlinear dispersion. We perform an autocorrelation with a pulse width of typically 10–12 fs, similar to the 8 fs measured by MIIPS. The slight discrepancy may relate to the three-pulse nature of the TG measurement and coherent nuclear response of the blank solvent [67]. All colors appear well compressed and the TG shows a flat, nearly symmetric profile.

This reflective delay method relies on angled stages and optical flats to generate precise time

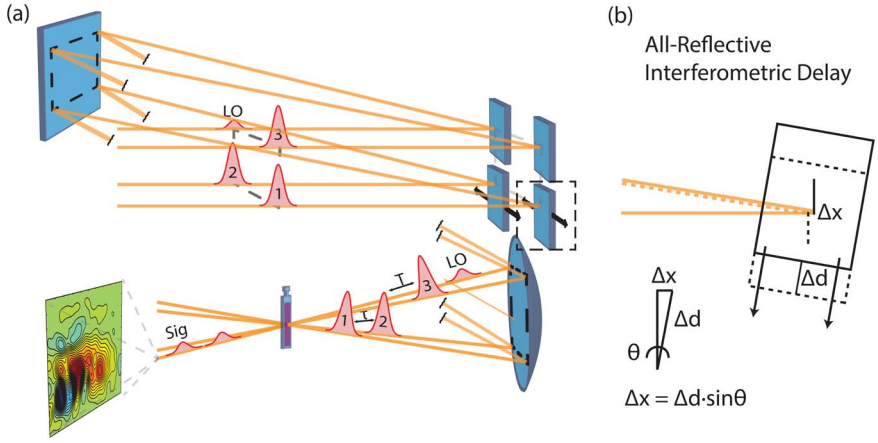

Fig. 7. (a) Three-dimensional representation of the apparatus. The coherence time is introduced and changed using reflective optics. (b) Detail of the coherence time control with angled stages. This design shows that for a parallel input, fine control can be achieved by propagating the stage at a very small angle (typically 0.3°).

delays. To separate incoming and outgoing beams, we angle each optic upward approximately 3.5° with respect to the table top [see Fig. 7(a)], which results in a small vertical displacement during delay. In our implementation, a 100 fs delay yields a positional deviation of ∼1 μm at the sample position. In Fig. 3(d), we show a comparison between the original TG signal and one in which beams 1 and 2 are delayed by 100 fs using an all-reflective delay system, while beam 3 is delayed using a mounted retroreflector that travels parallel to beam propagation. They show nearly identical response, illustrating minimal undesired side effects from adjusting the time delay.

We probe two different broadly absorbing systems, CdSe QDs in toluene and Chl a in methanol at 21°C. QD electronic structure and charge-carrier dynamics have been comprehensively reviewed elsewhere

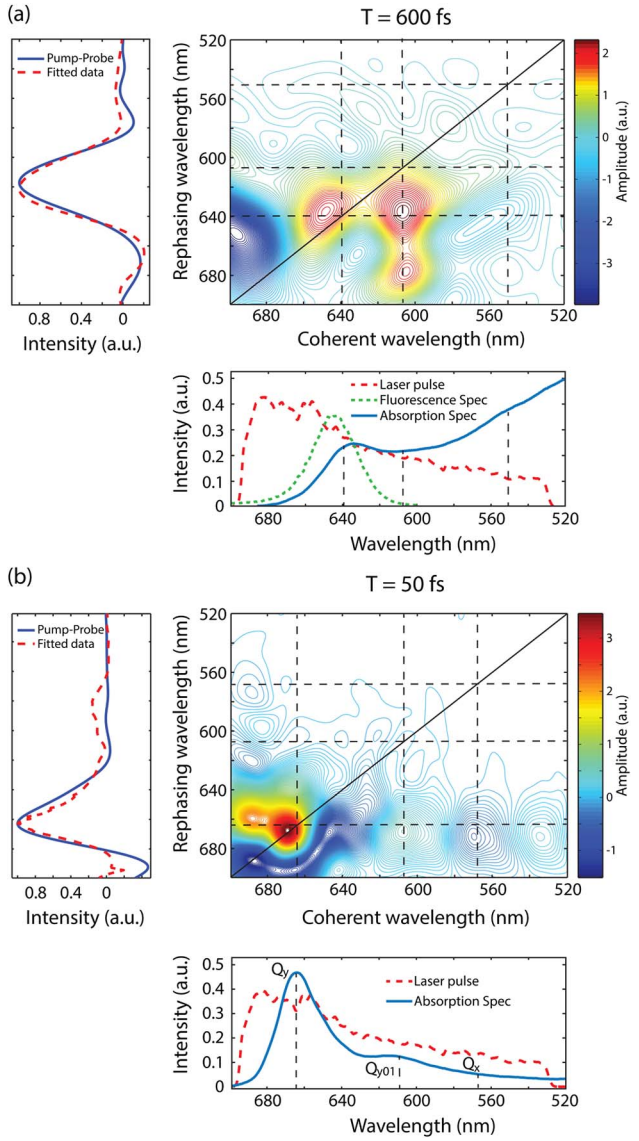

Fig. 8. Phased two-dimensional spectrum of (a) CdSe QDs at T = 600 fs and (b) Chl a at T = 50 fs. We plot the pump–probe spectra and the projected 2D spectra on the left. Below each spectrum, we plot the laser pulse and the linear absorption spectrum of each system.

[68–72]. Briefly, QDs have discrete electronic states at and near the band edge, which contribute to their optical nonlinear response. This electronic structure results in positive (stimulated emission/ground state bleach) and negative (excited state absorption) signatures, which can be probed to follow the electronic dynamics and the binding energy of biexcitons [73–77]. Previous 2D spectroscopy on QDs primarily focused on the band-edge exciton or the first two excitons, which are primarily associated with the lowest lying excited electronic state [16,78,79]. Recent work, however, has shown that the nonlinear response varies depending on which state is initially excited, with the largest difference occurring upon initial excitation into the 1P(e) higher lying electron manifold [61,80]. In Fig. 8(a), we show a 2D spectrum (combined nonrephasing and rephasing) of a relatively polydisperse sample of QDs (10% radial inhomogeneity). We observe significant differences in the nonlinear response depending on excitation energy, both in the position and sign of peaks. The ability to resolve frequencies of response domains enables us to probe detailed electronic dynamics despite the inhomogeneity of the ensemble.

To illustrate how C-2DES can be used to probe energy transfer in biological chromophores, we also generate phased 2D spectra of Chl a, as shown in Fig. 8(b). Here, we show distinct Q_y vibrational signals. The peak at 665 nm is assigned to the 0–0 transition of Q_y band, based on the linear absorption spectrum and other reports in similar polar organic solutions [81–83]. The peaks at 610, 565, and 525 nm may arise from other vibrational Q_y transitions, i.e., 0–0, 0–1, and even 0–2 transitions. These four peaks are almost evenly spaced in energy domain and consistent with previous reports [81,84]. The assignment of the Q_x band has not been straightforward [85,86]. Q_x bands have been observed at ∼570 nm [82,84] as well as at ∼620 nm [81,85,87]. Recent work to unify these assignments suggests that vibronic coupling can simultaneously explain all signals [86]. Similar to recent work on chlorophyll contained in the Photosystem I complex, we show little signal on the diagonal from the Q_x bands, but rather we see rapid growth of a cross peak between Q_x and Q_y at very early times [62]. The 2D spectra also show significant excited state absorption in this system, likely arising from excitation to higher lying electronic states [88].

4. Conclusion

In this work, white-light pulses are used to generate 2DES of CdSe QDs and Chl a. Using an all-reflective delay mechanism, we finely control the time delays without introducing phase nonlinearities. This method permits the use of broadband white-light pulses for all interactions. By fitting the 2D spectra using pump–probe data taken with the same laser pulse, we extract phased 2D spectra for both CdSe QDs and Chl a, showing highly complex 2D line

shapes, which will be explored more fully in future experiments.

The authors wish to thank Prof. Daniel Turner (NYU) for helpful guidance in our calculation of phase stability. The authors would like to thank NSF MRSEC (Grant No. DMR 08-02054), the Keck Foundation, and the AFOSR (Grant No. FA9550-09-1-0117), and DTRA (HDTRA1-10-1-0091) for supporting this work in part. J. R. C. and P. D. D. acknowledge support from the NSF GRFP. P. D. D. was supported by the Graduate Program in Biophysical Sciences at the University of Chicago (NIH Grant T32 Eb009412).

†These authors contributed equally to this work.

References

1. J. D. Hybl, A. A. Ferro, and D. M. Jonas, "Two-dimensional Fourier transform electronic spectroscopy," J. Chem. Phys. **115**, 6606–6622 (2001).
2. D. M. Jonas, "Two-dimensional femtosecond spectroscopy," Annu. Rev. Phys. Chem. **54**, 425–463 (2003).
3. M. L. Cowan, J. P. Ogilvie, and R. J. D. Miller, "Two-dimensional spectroscopy using diffractive optics based phased-locked photon echoes," Chem. Phys. Lett. **386**, 184–189 (2004).
4. T. Brixner, T. Mancal, I. Stiopkin, and G. Fleming, "Phase-stabilized two-dimensional electronic spectroscopy," J. Chem. Phys. **121**, 4221–4236 (2004).
5. K. Wells, Z. Zhang, J. Rouxel, and H. Tan, "Measuring the spectral diffusion of chlorophyll a using two-dimensional electronic spectroscopy," J. Phys. Chem. B **117**, 2294–2299 (2013).
6. J. D. Hybl, A. Yu, D. A. Farrow, and D. M. Jonas, "Polar solvation dynamics in the femtosecond evolution of two-dimensional Fourier transform spectra," J. Phys. Chem. A **106**, 7651–7654 (2002).
7. T. Brixner, J. Stenger, H. M. Vaswani, M. Cho, R. E. Blankenship, and G. R. Fleming, "Two-dimensional spectroscopy of electronic couplings in photosynthesis," Nature **434**, 625–628 (2005).
8. E. L. Read, G. S. Engel, T. R. Calhoun, T. Mancal, T. K. Ahn, R. E. Blankenship, and G. R. Fleming, "Cross-peak-specific two-dimensional electronic spectroscopy," Proc. Natl. Acad. Sci. USA **104**, 14203–14208 (2007).
9. E. Read, G. Engel, T. Calhoun, T. Mancal, T. Ahn, R. Blankenship, and G. Fleming, "Cross-peak-specific two-dimensional electronic spectroscopy," Proc. Natl. Acad. Sci. USA **104**, 14203–14208 (2007).
10. E. Collini, C. Y. Wong, K. E. Wilk, P. M. G. Curmi, P. Brumer, and G. D. Scholes, "Coherently wired light-harvesting in photosynthetic marine algae at ambient temperature," Nature **463**, 644–647 (2010).
11. G. Schlau-Cohen, A. Ishizaki, and G. Fleming, "Two-dimensional electronic spectroscopy and photosynthesis: fundamentals and applications to photosynthetic light-harvesting," Chem. Phys. **386**, 1–22 (2011).
12. N. Ginsberg, J. Davis, M. Ballottari, Y. Cheng, R. Bassi, and G. Fleming, "Solving structure in the CP29 light harvesting complex with polarization-phased 2D electronic spectroscopy," Proc. Natl. Acad. Sci. USA **108**, 3848–3853 (2011).
13. E. Harel and G. S. Engel, "Quantum coherence spectroscopy reveals complex dynamics in bacterial light-harvesting complex 2 (LH2)," Proc. Natl. Acad. Sci. USA **109**, 706–711 (2012).
14. E. E. Ostroumov, R. M. Mulvaney, R. J. Cogdell, and G. D. Scholes, "Broadband 2D electronic spectroscopy reveals a carotenoid dark state in purple bacteria," Science **340**, 52–56 (2013).
15. G. Moody, R. Singh, H. Li, I. A. Akimov, M. Bayer, D. Reuter, A. D. Wieck, A. S. Bracker, D. Gammon, and S. T. Cundiff, "Influence of confinement on biexciton binding in semiconductor quantum dot ensembles measured with two-dimensional spectroscopy," Phys. Rev. B **87**, 041304 (2013).
16. C. Wong and G. Scholes, "Biexcitonic fine structure of CdSe nanocrystals probed by polarization-dependent two-dimensional photon echo spectroscopy," J. Phys. Chem. A **115**, 3797–3806 (2011).
17. D. Turner, Y. Hassan, and G. Scholes, "Exciton superposition states in CdSe nanocrystals measured using broadband two-dimensional electronic spectroscopy," Nano Lett. **12**, 880–886 (2012).
18. G. Griffin, S. Ithurria, D. Dolzhnikov, A. Linkin, D. Talapin, and G. Engel, "Two-dimensional electronic spectroscopy of CdSe nanoparticles at very low pulse power," J. Chem. Phys. **138**, 014705 (2013).
19. P. Tian, D. Keusters, Y. Suzaki, and W. S. Warren, "Femtosecond phase-coherent two-dimensional spectroscopy," Science **300**, 1553–1555 (2003).
20. X. Dai, A. Bristow, D. Karaiskaj, and S. Cundiff, "Two-dimensional Fourier-transform spectroscopy of potassium vapor," Phys. Rev. A **82**, 052503 (2010).
21. P. F. Tekavec, G. A. Lott, and A. H. Marcus, "Fluorescence-detected two-dimensional electronic coherence spectroscopy by acousto-optic phase modulation," J. Chem. Phys. **127**, 214307 (2007).
22. H. Li, A. D. Bristow, M. E. Siemens, G. Moody, and S. T. Cundiff, "Unraveling quantum pathways using optical 3d Fourier-transform spectroscopy," Nat. Commun. **4**, 1390 (2013).
23. M. Cho, "Coherent two-dimensional optical spectroscopy," Chem. Rev. **108**, 1331–1418 (2008).
24. J. Hybl, A. Albrecht, S. Faeder, and D. Jonas, "Two-dimensional electronic spectroscopy," Chem. Phys. Lett. **297**, 307–313 (1998).
25. M. Cho, *Two-dimensional Optical Spectroscopy* (CRC Press, 2009).
26. R. N. Augulis and D. Zigmantas, "Detector and dispersive delay calibration issues in broadband 2D electronic spectroscopy," J. Opt. Soc. Am. B **30**, 1770–1774 (2013).
27. J. A. Davis, T. R. Calhoun, K. A. Nugent, and H. M. Quiney, "Ultrafast optical multidimensional spectroscopy without interferometry," J. Chem. Phys. **134**, 024504 (2011).
28. Y. Zhang, K. Meyer, C. Ott, and T. Pfeifer, "Passively phase-stable, monolithic, all-reflective two-dimensional electronic spectroscopy based on a four-quadrant mirror," Opt. Lett. **38**, 356–358 (2013).
29. U. Selig, C. F. Schleussner, M. Foerster, F. Langhojer, P. Nuernberger, and T. Brixner, "Coherent two-dimensional ultraviolet spectroscopy in fully noncollinear geometry," Opt. Lett. **35**, 4178–4180 (2010).
30. U. Selig, F. Langhojer, F. Dimler, T. Lohrig, C. Schwarz, B. Gieseking, and T. Brixner, "Inherently phase-stable coherent two-dimensional spectroscopy using only conventional optics," Opt. Lett. **33**, 2851–2853 (2008).
31. T. Zhang, C. Borca, X. Li, and S. Cundiff, "Optical two-dimensional Fourier transform spectroscopy with active interferometric stabilization," Opt. Express **13**, 7432–7441 (2005).
32. E. Harel, A. Fidler, and G. Engel, "Real-time mapping of electronic structure with single-shot two-dimensional electronic spectroscopy," Proc. Natl. Acad. Sci. USA **107**, 16444–16447 (2010).
33. E. Harel, A. Fidler, and G. Engel, "Single-shot gradient-assisted photon echo electronic spectroscopy," J. Phys. Chem. A **115**, 3787–3796 (2011).
34. D. B. Turner, K. W. Stone, K. Gundogdu, and K. A. Nelson, "Invited article: the coherent optical laser beam recombination technique (colbert) spectrometer: coherent multidimensional spectroscopy made easier," Rev. Sci. Instrum. **82**, 081301 (2011).
35. S. Yin, O. Leonov, F. Yu, V. Molotok, and V. Kludzin, "Design and fabrication of a 24-channel acousto-optic spatial light modulator," Appl. Opt. **37**, 7482–7489 (1998).
36. S.-H. Shim, D. B. Strasfeld, Y. L. Ling, and M. T. Zanni, "Automated 2D IR spectroscopy using a mid-IR pulse shaper and application of this technology to the human islet amyloid polypeptide," Proc. Natl. Acad. Sci. USA **104**, 14197–14202 (2007).

37. J. Myers, K. Lewis, P. Tekavec, and J. Ogilvie, "Two-color two-dimensional Fourier transform electronic spectroscopy with a pulse-shaper," Opt. Express **16**, 17420–17428 (2008).
38. P. Tyagi, J. I. Saari, B. Walsh, A. Kabir, V. Crozatier, N. Forget, and P. Kambhampati, "Two-color two-dimensional electronic spectroscopy using dual acousto-optic pulse shapers for complete amplitude, phase, and polarization control of femtosecond laser pulses," J. Phys. Chem. A **117**, 6264–6269 (2013).
39. K. Iizuka, *Elements of Photonics* (Wiley-Interscience, 2002).
40. B. A. West, B. P. Molesky, P. G. Giokas, and A. M. Moran, "Uncovering molecular relaxation processes with nonlinear spectroscopies in the deep UV," Chem. Phys. **423**, 92–104 (2013).
41. E. Harel, P. D. Long, and G. S. Engel, "Single-shot ultrabroadband two-dimensional electronic spectroscopy of the light-harvesting complex LH2," Opt. Lett. **36**, 1665–1667 (2011).
42. D. E. Wilcox, F. D. Fuller, and J. P. Ogilvie, "Fast second-harmonic generation frequency-resolved optical gating using only a pulse shaper," Opt. Lett. **38**, 2980–2983 (2013).
43. D. Kartashov, S. Aliauskas, A. Puglys, A. Voronin, A. Zheltikov, M. Petrarca, P. Béjot, J. Kasparian, J.-P. Wolf, and A. Baltuka, "White light generation over three octaves by femtosecond filament at 3.9 μm in argon," Opt. Lett. **37**, 3456–3458 (2012).
44. M. Nisoli, S. DeSilvestri, and O. Svelto, "Generation of high energy 10 fs pulses by a new pulse compression technique," Appl. Phys. Lett. **68**, 2793–2795 (1996).
45. M. Nisoli, G. Sansone, S. Stagira, C. Vozzi, S. De Silvestri, and O. Svelto, "Ultra-broadband continuum generation by hollow-fiber cascading," Appl. Phys. B **75**, 601–604 (2002).
46. G. Steinmeyer and G. Stibenz, "Generation of sub-4-fs pulses via compression of a white-light continuum using only chirped mirrors," Appl. Phys. B **82**, 175–181 (2006).
47. H. Wang, Y. Wu, C. Li, H. Mashiko, S. Gilbertson, and Z. Chang, "Generation of 0.5 mJ, few-cycle laser pulses by an adaptive phase modulator," Opt. Express **16**, 14448–14455 (2008).
48. K. Yamane, Z. Zhang, K. Oka, R. Morita, M. Yamashita, and A. Suguro, "Optical pulse compression to 3.4 fs in the monocycle region by feedback phase compensation," Opt. Lett. **28**, 2258–2260 (2003).
49. B. Xu, Y. Coello, V. Lozovoy, D. Harris, and M. Dantus, "Pulse shaping of octave spanning femtosecond laser pulses," Opt. Express **14**, 10939–10944 (2006).
50. B. Xu, J. Gunn, J. Dela Cruz, V. Lozovoy, and M. Dantus, "Quantitative investigation of the multiphoton intrapulse interference phase scan method for simultaneous phase measurement and compensation of femtosecond laser pulses," J. Opt. Soc. Am. B **23**, 750–759 (2006).
51. R. Trebino, K. DeLong, D. Fittinghoff, J. Sweetser, M. Krumbugel, B. Richman, and D. Kane, "Measuring ultrashort laser pulses in the time-frequency domain using frequency-resolved optical gating," Rev. Sci. Instrum. **68**, 3277–3295 (1997).
52. R. Trebino, *Frequency-Resolved Optical Gating: The Measurement of Ultrashort Laser Pulses* (Springer, 2002).
53. J. Sweetser, D. Fittinghoff, and R. Trebino, "Transient-grating frequency-resolved optical gating," Opt. Lett. **22**, 519–521 (1997).
54. N. Christensson, F. Milota, J. Hauer, J. Sperling, O. Bixner, A. Nemeth, and H. F. Kauffmann, "High frequency vibrational modulations in two-dimensional electronic spectra and their resemblance to electronic coherence signatures," J. Phys. Chem. B **115**, 5383–5391 (2011).
55. D. B. Turner, K. E. Wilk, P. M. G. Curmi, and G. D. Scholes, "Comparison of electronic and vibrational coherence measured by two-dimensional electronic spectroscopy," J. Phys. Chem. Lett. **2**, 1904–1911 (2011).
56. M. K. Yetzbacher, N. Belabas, K. A. Kitney, and D. M. Jonas, "Propagation, beam geometry, and detection distortions of peak shapes in two-dimensional Fourier transform spectra," J. Chem. Phys. **126**, 044511 (2007).
57. C. Dorrer, N. Belabas, J. P. Likforman, and M. Joffre, "Spectral resolution and sampling issues in Fourier-transform spectral interferometry," J. Opt. Soc. Am. B **17**, 1795–1802 (2000).
58. S. Mukamel, *Principles of Nonlinear Optical Spectroscopy* (Oxford, 1995).
59. A. Zewail, "Femtochemistry: atomic-scale dynamics of the chemical bond," J. Phys. Chem. A **104**, 5660–5694 (2000).
60. M. Drescher, M. Hentschel, R. Kienberger, M. Uiberacker, V. Yakovlev, A. Scrinzi, T. Westerwalbesloh, U. Kleineberg, U. Heinzmann, and F. Krausz, "Time-resolved atomic inner-shell spectroscopy," Nature **419**, 803–807 (2002).
61. P. Kambhampati, "Hot exciton relaxation dynamics in semiconductor quantum dots: radiationless transitions on the nanoscale," J. Phys. Chem. C **115**, 22089–22109 (2011).
62. J. Anna, E. Ostroumov, K. Maghlaoui, J. Barber, and G. Scholes, "Two-dimensional electronic spectroscopy reveals ultrafast downhill energy transfer in photosystem I trimers of the Cyanobacterium *Thermosynechococcus elongatus*," J. Phys. Chem. Lett. **3**, 3677–3684 (2012).
63. J. Du, K. Nakata, Y. Jiang, E. Tokunaga, and T. Kobayashi, "Spectral modulation observed in Chl-a by ultrafast laser spectroscopy," Opt. Express **19**, 22480–22485 (2011).
64. V. I. Prokhorenko, A. Halpin, and R. J. D. Miller, "Coherently-controlled two-dimensional photon echo electronic spectroscopy," Opt. Express **17**, 9764–9779 (2009).
65. G. Panitchayangkoon, D. Hayes, K. Fransted, J. Caram, E. Harel, J. Wen, R. Blankenship, and G. Engel, "Long-lived quantum coherence in photosynthetic complexes at physiological temperature," Proc. Natl. Acad. Sci. USA **107**, 12766–12770 (2010).
66. P. F. Tekavec, J. A. Myers, K. L. M. Lewis, F. D. Fuller, and J. P. Ogilvie, "Effects of chirp on two-dimensional Fourier transform electronic spectra," Opt. Express **18**, 11015–11024 (2010).
67. M. Li, J. P. Nibarger, C. Guo, and G. N. Gibson, "Dispersion-free transient-grating frequency-resolved optical gating," Appl. Opt. **38**, 5250–5253 (1999).
68. A. L. Efros and M. Rosen, "The electronic structure of semiconductor nanocrystals," Annu. Rev. Mater. Sci. **30**, 475–521 (2000).
69. D. Norris and M. Bawendi, "Measurement and assignment of the size-dependent optical spectrum in CdSe quantum dots," Phys. Rev. B **53**, 16338–16346 (1996).
70. V. I. Klimov, D. W. McBranch, C. A. Leatherdale, and M. G. Bawendi, "Electron and hole relaxation pathways in semiconductor quantum dots," Phys. Rev. B **60**, 13740–13749 (1999).
71. V. I. Klimov, "Optical nonlinearities and ultrafast carrier dynamics in semiconductor nanocrystals," J. Phys. Chem. B **104**, 6112–6123 (2000).
72. V. I. Klimov, "Spectral and dynamical properties of multiexcitons in semiconductor nanocrystals," Annu. Rev. Phys. Chem. **58**, 635–673 (2007).
73. S. L. Sewall, A. Franceschetti, R. R. Cooney, A. Zunger, and P. Kambhampati, "Direct observation of the structure of band-edge biexcitons in colloidal semiconductor CdSe quantum dots," Phys. Rev. B **80**, 081310 (2009).
74. G. D. Scholes, "Selection rules for probing biexcitons and electron spin transitions in isotropic quantum dot ensembles," J. Chem. Phys. **121**, 10104 (2004).
75. S. L. Sewall, R. R. Cooney, K. E. H. Anderson, E. A. Dias, D. M. Sagar, and P. Kambhampati, "State-resolved studies of biexcitons and surface trapping dynamics in semiconductor quantum dots," J. Chem. Phys. **129**, 084701 (2008).
76. K. W. Stone, K. Gundogdu, D. B. Turner, X. Li, S. T. Cundiff, and K. A. Nelson, "Two-quantum 2D FT electronic spectroscopy of biexcitons in GaAs quantum wells," Science **324**, 1169–1173 (2009).
77. P. Kambhampati, "Unraveling the structure and dynamics of excitons in semiconductor quantum dots," Acc. Chem. Res. **44**, 1–13 (2011).
78. D. B. Turner, Y. Hassan, and G. D. Scholes, "Exciton superposition states in CdSe nanocrystals measured using broadband two-dimensional electronic spectroscopy," Nano Lett. **12**, 880–886 (2012).
79. C. Y. Wong and G. D. Scholes, "Using two-dimensional photon echo spectroscopy to probe the fine structure of the ground state biexciton of CdSe nanocrystals," J. Lumin. **131**, 366–374 (2011).

80. P. Kambhampati, "Multiexcitons in semiconductor nanocrystals: a platform for optoelectronics at high carrier concentration," J. Phys. Chem. Lett. **3**, 1182–1190 (2012).
81. M. Ratsep, J. Linnanto, and A. Freiberg, "Mirror symmetry and vibrational structure in optical spectra of Chlorophyll a," J. Chem. Phys. **130**, 194501 (2009).
82. R. E. Blankenship, *Molecular Mechanisms of Photosynthesis* (Blackwell Science, 2002).
83. J. Du, T. Teramoto, K. Nakata, E. Tokunaga, and T. Kobayashi, "Real-time vibrational dynamics in Chlorophyll a studied with a few-cycle pulse laser," Biophys. J. **101**, 995–1003 (2011).
84. J. L. Hughes, B. Conlon, T. Wydrzynski, and E. Krausz, "The assignment of $Q_y(1,0)$ vibrational structure and Q_x for Chlorophyll a," Phys. Proc. **3**, 9 (2010).
85. I. Renge, K. Mauring, P. Sarv, and R. Avarmaa, "Vibrationally resolved optical-spectra of chlorophyll derivatives in different solid media," J. Phys. Chem. **90**, 6611–6616 (1986).
86. J. R. Reimers, Z. L. Cai, R. Kobayashi, M. Ratsep, A. Freiberg, and E. Krausz, "Assignment of the Q-bands of the chlorophylls: coherence loss via Q_x—Q_y mixing," Sci. Rep. **3**, 2761 (2013).
87. M. Umetsu, Z. Y. Wang, M. Kobayashi, and T. Nozawa, "Interaction of photosynthetic pigments with various organic solvents—magnetic circular dichroism approach and application to chlorosomes," Biochim. Biophys. Acta **1410**, 19–31 (1999).
88. L. De Boni, D. S. Correa, F. J. Pavinatto, D. S. dos Santos, and C. R. Mendonca, "Excited state absorption spectrum of chlorophyll a obtained with white-light continuum," J. Chem. Phys. **126**, 165102 (2007).